European Journal of Pharmacology 969 (2024) 176453

Contents lists available at ScienceDirect

European Journal of Pharmacology

journal homepage: www.elsevier.com/locate/ejphar

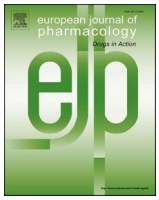

Tyrosol attenuates NASH features by reprogramming the hepatic immune milieu

Daniela Gabbia [a], Katia Sayaf [b], Ilaria Zanotto [a], Martina Colognesi [a], Yahima Frion-Herrera [a], Maria Carrara [a], Francesco Paolo Russo [b], Sara De Martin [a,*]

[a] Department of Pharmaceutical and Pharmacological Sciences, University of Padova, Padova, Italy
[b] Department of Surgery, Oncology and Gastroenterology, University of Padova, Padova, Italy

ARTICLE INFO

Keywords:
NAFLD
NASH
Tyrosol
Oxidative stress
Inflammation
Fibrosis
Steatosis
Steatotic liver disease
MASLD
MASH

ABSTRACT

Nonalcoholic steatohepatitis (NASH) is a leading cause of chronic liver disease, and no drugs have been approved for its therapy. Among plant-derived molecules, phenolic compounds of extra virgin olive oil like tyrosol (Tyr) had demonstrated multiple beneficial actions for liver health, including the modulation of inflammation in fibrosis. This study aims at assessing the protective effect and mechanism of Tyr in *in vitro* and *in vivo* models of NASH, with a focus on the hepatic immune microenvironment and extrahepatic manifestations. The effect of Tyr was evaluated in cellular models of NASH, obtained by co-culturing palmitic and oleic acid-treated HepG2 cells with THP1-derived M1 macrophages and LX2 cells, and in a mouse model of NASH induced by a high fructose-high fat diet combined to CCl_4 treatment. *In vitro* Tyr reduced fatty acid (FA) accumulation in HepG2 cells and displayed a beneficial effect on LX2 activation and macrophage differentiation. *In vivo*, beside reducing steatosis and fibrosis in NASH animals, Tyr prevented inflammation, as demonstrated by the reduction of hepatic inflammatory foci, and immune cells like $CD86^+$ macrophages ($p < 0.05$), $CD4^+$ ($p < 0.05$) and T helper effector $CD4^+$ $FoxP3^-$ $CD62L^-$lymphocytes ($p < 0.05$). Also, the prooxidant enzyme NOX1 and the mRNA expression of TGF-β1 and IL6 ($p < 0.05$) were reduced by Tyr. Notably, in Tyr-treated animals, a significant increase of $CD4^+$ $FoxP3^+$ T_{reg} cells ($p < 0.05$) was observed, involved in regenerative pathways. Moreover, Tyr attenuated the fatigue and anxious behavior observed in NASH mice. In conclusion, Tyr effectively reduced NASH-related steatosis, fibrosis, oxidative stress, and inflammation, displaying a beneficial effect on the hepatic immune infiltrate, indicating its possible development as a therapeutic agent for NASH due to its multifaceted mechanism.

1. Introduction

Nonalcoholic steatohepatitis (NASH) is a leading cause of chronic liver disease and the second indication for liver transplantation in the United States (Estes et al., 2018; Younossi et al., 2019, 2021). This progressive liver disease represents the main complication of non-alcoholic fatty liver disease (NAFLD), which was recently renamed as metabolic dysfunction-associated steatotic liver disease (MASLD). This new definition, at variance with NAFLD, is affirmative and non-stigmatizing. NASH is commonly associated with other manifestations of the metabolic syndrome, e.g. obesity, insulin resistance and diabetes, and is responsible for an increase of liver disease-related morbidity and mortality (Majzoub et al., 2021). Its progression can lead to cirrhosis and hepatocellular carcinoma (HCC) (Rinella et al., 2023). The estimated annual incidence of HCC ranges from 0.5% to 2.6% among cirrhotic patients with NASH (Huang et al., 2021; Rinella et al., 2023). NASH and NASH-related cirrhosis displayed a growing incidence in the last years, due to the increase of obesity and diabetes mostly in developed countries. Notably, also the new cases of NASH-related HCC are increased worldwide.

Even though several drug candidates have caused significant improvements in the histological features of NASH during Phase 2b and Phase 3 trials, and some molecules are currently under evaluation in various phases of clinical development, regulatory agencies (FDA and EMA) have not yet approved a drug for the treatment of NASH, which still represents a major clinical challenge (Pearlman and Loomba, 2014). Drug approval for NASH is challenging. In general, the monotherapies tested so far seem to exert a small effect on disease features, not always relevant when compared to the placebo group. Therefore, a recent meta-analysis suggested that future effective therapies may rely on the

* Corresponding author. L.go Meneghetti, 2, 35131, Padova, Italy.
E-mail address: sara.demartin@unipd.it (S. De Martin).

https://doi.org/10.1016/j.ejphar.2024.176453
Received 22 August 2023; Received in revised form 14 February 2024; Accepted 20 February 2024
Available online 24 February 2024

combination of selected molecules with anti-fibrotic drugs or other agents with beneficial effect on liver health to boost treatment response rate (Majzoub et al., 2021). At present, lifestyle interventions remain the current mainstay of NASH patients' management (Dong et al., 2023). These interventions include dietary caloric restriction, increased physical activity and adoption of a healthy diet (Chalasani et al., 2018).

Tyrosol [Tyr, 2-(4-hydroxyphenyl)-ethanol] is the most abundant phenolic compound present in extra virgin olive oil (EVOO), one of the pillar of Mediterranean diet, and the main bioactive component of *Rhodiola rosea*, a plant extensively used in the traditional Chinese medicine (Cui et al., 2016). Notably *Rhodiola rosea* has been studied in preclinical models of MASLD/NASH for its multiple positive actions, e.g. improvement of dysfunctional lipid metabolism and fibrosis, inhibition of oxidative stress, mitigation of inflammatory response, and regulation of gut microbiota, although these effects have been mainly imputed to salidroside, the main phenolic glycoside compound of this plant (Qu et al., 2022).

Numerous studies reported that Tyr is able to exert a broad range of biological effects, including for example antioxidant, antiapoptotic effects and a convincing anti-inflammatory action, targeting different organs (Mateos et al., 2020). For example, previous studies demonstrated that Tyr improved inflammatory lung diseases *via* the inhibition of inflammatory responses and the integrity maintenance of alveolar capillary barrier (Kim et al., 2017). Furthermore, Tyr reduced lipopolysaccharide-induced inflammation in HUVEC cells, suggesting its protective role in vascular health promotion and atherosclerosis prevention (Zhao et al., 2023). Moreover, Tyr has been described as a pan-pro-inflammatory cytokine inhibitor, acting on TNF-α, IL-1β, IL-6 and iNOS and reducing NF-κB activation (Paramita Pal et al., 2023). However, only limited information is available on the effect of Tyr in the liver, mostly demonstrating a positive effect on NAFLD due to the modulation of oxidative stress-related enzymes and JAK1/STAT3 pathway (Huang et al., 2022; Sarna et al., 2016). Even though our previous study observed a positive effect also on fibrosis (Gabbia et al., 2023), no studies have investigated the effect of tyrosol on NASH, a complex disease in which steatosis, low grade inflammation and fibrosis concurrently affect the liver, and on its extrahepatic manifestations, e.g. motorial dysfunction, anxiety or depressive-like behavior. Moreover, nothing is available to date on its possible effect on the phenotype of the immune cells constituting the microenvironment of solid organs, including the liver.

In the light of these considerations, this study aimed at assessing the potential antifibrotic, antisteatotic and anti-inflammatory effects of Tyr in different preclinical models of NASH. We performed our investigations in vitro, on 2D and 3D cellular models, and on a mouse *in vivo* model. To gain insight in Tyr mechanism, we focused on the modulation of hepatic immune microenvironment. Furthermore, we implemented the study by investigating its effect on some extrahepatic manifestations of NASH, including motorial dysfunction, depressive-like behavior, and anxiety.

2. Materials and methods

2.1. Chemicals and cell lines

Dulbecco's modified eagle medium (DMEM), Roswell Park Memorial Institute (RPMI) medium, Dulbecco's phosphate-buffered saline (DPBS), Streptomycin-penicillin 100X, trypsin-EDTA, L-glutamine, matrigel matrix and fetal bovine serum (FBS) were purchased from Corning (Corning, NY, USA). 2′,7′-diclorofluorescin diacetate (H_2DCF-DA), Palmitic acid (PA), oleic acid (OA) and Tyr were purchased from Sigma Aldrich (St. Luis, MO, USA). A 50 mM stock solution of PA:OA 1:2 was prepared and stored at 4 °C in the dark. Tyr was dissolved in DMSO at 50 mM and stored at −20 °C. Phorbol 12-myristate 13-acetate (PMA) was purchased from Santa Cruz Biotechnology, USA).

Human HepG2 and LX2 cells were maintained in a DMEM complete medium, containing L-glutamine (1%), streptomycin/penicillin (1%) and 10% or 3% FBS, respectively. THP-1 monocyte-like cells were maintained in a RPMI complete medium, containing L-glutamine (1%), streptomycin/penicillin (1%) and 10% FBS. All cell lines were grown at 37 °C with 5% CO_2 in humified atmosphere. Antibodies: mouse monoclonal anti-αSMA antibody (Cell Marque, Sigma-Aldrich, Darmstadt, GE), rabbit polyclonal anti-NOX1 antibody (GeneTex, Alton Pkwy Irvine, CA), goat anti-rabbit HRP-conjugated IgG (KPL, Gaithersburg, MD) and goat anti-mouse HRP-conjugated IgG (Abcam, Cambridge, UK).

Masson trichrome, O Red Oil and H&E stain, 3,3′-diaminobenzidine (DAB) substrate for HRP-conjugated antibodies and EUKITT® Quick-hardening mounting medium were purchased from Sigma-Aldrich (St. Luis, MO, USA).

2.2. Effect of tyr in an in vitro 2D model of steatosis

HepG2 cells were seeded in a 24-well plate on glass coverslips a density of 20,000 cell/mL. To stimulate the accumulation of fatty acids inside hepatocytes, as typically occurring in NAFLD, HepG2 cells were treated for 24h with a PA:OA 1:2 mixture (100 μM) in absence (control) or presence of increasing concentration (0.5, 1, 2 and 5 μM) of Tyr, diluted in complete cell culture medium.

At the end of the treatment, cells were fixed with PFA for 20 min at RT, permeabilized with 0.1% Triton X100 in PBS for 10 min, and then treated with 5% FBS in PBS for 10 min and stained with Bodipy 493/503 (1:1000 Thermo Fisher) for 1 h at RT. Nuclei were counterstained with Hoechst 33,342 (1:500 in PBS, Thermo Fisher) and mounted with mowiol. Cell images were acquired by means of a T-lapse confocal microscope Zeiss LSM 800 (Zeiss, Milano, Italy) and quantified with the ImageJ software.

To analyze reactive oxygen species (ROS) production, the DCFDA assay was used, using a previously reported protocol (Frión-Herrera et al., 2019). Briefly, after being seeded into 96-black well plates, HepG2 cells treated with the PA:OA mixture for 24 h in absence or presence of Tyr, were incubated with 10 μM H_2DCF-DA for 30 min, HepG2 cells incubated with H_2O_2 0.5% for 30 min were used as positive control. Fluorescence intensity (excitation lambda = 495 nm; emission lambda = 530 nm) was measured using a Victor Nivo multiplate reader (PerkinElmer). The results are reported as DCFDA fluorescence intensity (AU) normalized on cell number in each well.

2.3. Effect of tyr in an in vitro 2D model of steatosis and inflammation

A coculture of HepG2 and THP-1-derived macrophages with the M1 proinflammatory phenotype was used to simulate steatosis in presence of a proinflammatory microenvironment. THP1 monocytes were seeded on transwells with porous membranes (0.4 μm Falcon® pores, Corning Incorporated, USA) at a density of 50,000 cells/mL and treated for 24 h with 320 nM PMA, interferon-gamma (INFγ, Sigma Aldrich, USA) at 20 ng/mL and LPS (Sigma Aldrich, USA) at 100 ng/mL in order to obtain the pro-inflammatory M1 macrophages (*Frión-Herrera* et al., *2020a*). The co-culture was set up, transwells with the M1 macrophages were placed on 24-well plates in which HepG2 cells were seeded at a density of 20,000 cells/mL. The coculture was treated for 24 h with PA:OA as reported above, in absence or presence of increasing concentrations (0.5, 1, 2 and 5 μM) of Tyr diluted in complete medium. At the end of the treatment, HepG2 cells were stained with Bodipy 493/503 as above reported to analyze lipid droplets.

2.4. Effect of tyr in an in vitro multicellular spheroid model

A 3D multicellular spheroid (MCS) model was set up by seeding HepG2 and LX2 cells (1:1) in a 96-well round bottom ultra-low attachment (ULA) microplates (BIOFLOAT™) at 4×10^3 cells/well, incubated at 37 °C for 48–72 h to allow spheroid formation. Meanwhile, THP1

monocytes were treated for 24 h with 320 nM of PMA to obtain Mφ macrophages (Frión-Herrera et al., 2020b). Then, THP1-derived Mφ macrophages were overlayed on MCSs at 1:1 ratio. The so-formed MSC was treated with the PA:OA 1:2 mixture (100 μM) in absence or presence of Tyr (2 and 5 μM) for 24 h. MSC morphology and cell viability were assessed by a bright field microscope and CellTiter-Glo® Luminescent Cell Viability Assay kit (Promega), respectively. At the end of the treatment, MCS were stained with 1 μg/mL Nile Red in PBS for 1 h in the dark at RT, washed with PBS and examined immediately at the confocal microscope. All images were analyzed using the ImageJ software. ImageJ parameter "Circularity" (Cir) was used to calculate the Sphericity Index (SI): $SI = \sqrt{Cir}$, determining the proximity of the spheroids to a spherical geometry shape (Kelm et al., 2003). MCS volume was determined by ReViSP (MATLAB©, The MathWorks, Inc., MA, USA) (Piccinini et al., 2015).

2.5. Effect of tyr on macrophage polarization in the MCS

The effect of Tyr on polarization of THP1-derived M0 macrophages in coculture with the MCS described above was assessed after 24h-treatment with 2 and 5 μM Tyr. MSCs were fixed with 4% PFA, washed with PBS and incubated with 0.1% Triton X-100 in PBS for 5 min. Afterwards, they were incubated with the mouse anti-CD68 (1:200) and rabbit anti-CD86 (1:200) primary antibodies at 4 °C overnight. Subsequently, the fixed MCSs were incubated with AlexaFluor647 goat anti-rabbit IgG and AlexaFluor 488 anti-mouse IgG secondary antibody (1:200) for 1 h at RT in the dark. The nuclear DNA was stained with Hoechst33342 (1:400). The images were acquired using confocal microscope, capturing at least 50 consecutive focal planes for each spheroid, and quantified with the Image J software. Mean fluorescence intensity for each spheroid was plotted with GraphPad Prism software ver. 9.0 (San Diego, CA, USA).

2.6. Effect of tyr on LX-2 activation in the MCS

The effect of Tyr on activation of LX2 cells, cell line with the characteristics of hepatic stellate cells, which are activated during fibrogenesis, was assessed after 24h-treatment with 2 and 5 μM Tyr. MCS were fixed with 4% PFA, washed with PBS and incubated with 0.1% Triton X-100 in PBS for 5 min. Afterwards, they were incubated with the mouse anti-Acta2 (1:200) primary antibody at 4 °C overnight. Subsequently, fixed MCS were incubated with the AlexaFluor647 goat anti-rabbit IgG secondary antibody (1:200, 1h, RT) in the dark. The nuclear DNA was stained with Hoechst33342 (1:400). The images were acquired at the confocal microscope and analyzed with the Image J software as above described.

2.7. Effect of tyr in a mouse model of NASH

Animal studies were performed following the 3R principle, in compliance with national and international guidelines for the handling and use of laboratory animals (authorized by the Italian Ministry of Health, Approval no. 713/2020-PR). Male C57Bl6 mice (6 ± 2 weeks) were housed in a controlled temperature and humidity room with a 12h-light-dark cycle. They were randomized into the experimental groups (Fig. 1) and fed with standard rodent diet (Altromin, Lage, Germany) or a high fat diet (HFD: 60% Kcal from fat, 23.5% from protein, 18.4% from carbohydrates, Altromin, Lage, Germany) with 30% fructose in the drinking water (High fat high fructose diet, HFHFD) for 14 weeks. Mice had free access to diet and water along the complete duration of the study. During the last 4 weeks, the animals fed with HFHFD were treated with CCl_4 twice a week (IP, 0.1 mL/kg) to induce NAFLD progression to NASH (Zhang et al., 2020). Tyr (10 mg/kg) was administered daily by oral gavage starting from week 4, for the following 10 weeks. Standard diet-fed mice were used as healthy controls. At sacrifice, mice were anesthetized and perfused with saline solution by hearth cannulation to eliminate blood. The livers were collected, minced, nitrogen frozen and either stored at −80 °C for molecular biology, or kept in saline solution for flow cytometry analysis, or fixed in 4% neutral buffered formalin (Sigma Aldrich, MO, USA) for histology.

2.8. Behavioral tests

All the behavioral tests described in detail below were performed at week 14, before sacrifice.

Gripping test: The Gripping test was used to measure the muscle strength of mouse forelimbs. Briefly, mice were gently positioned on the grid and pulled backwards by the tail. The force was recorded by a dynamometer connected to the grid and expressed in Newtons. Data are reported as the mean of three consecutive measures for each mouse.

Grid tests: The Grid test evaluates muscle strength and coordination by testing the ability of mice to hang on a wire mesh screen grid (Deacon, 2013). Each mouse was placed in the center of a square metal grid which was then turned upside down. The time during which the mouse remained hanged on the grid was recorded. When the mouse fall, it was returned to the center of the grid and the experiment was repeated until the mice showed visible signs of weakness or distress, no longer than 15 min. The mean time hanged on the grid was used to calculate physical impulse expressed as grams of body weight * seconds on the grid.

Rotarod test: The Rotarod test was used to evaluate coordination and resistance to fatigue. The animals were placed on a rotating cylinder for up to 3 min, and the time elapsed before falling from the cylinder was evaluated. Three consecutive measurements were made per mouse (Deacon, 2013).

Open field test: The Open field test was used to evaluate the level of anxiety of the mice. The test was preceded by an hour of habituation, during which the animal was moved to a different room both from the usual housing and from the one set up for the experiment. At the end of the habituation, the mice were placed in a corner inside a square arena with dark walls of the size of 40 cm^3. Behavior in reaction to the new environment and movements within the central and peripheral areas were recorded for 10 min (Kraeuter et al., 2019). Total distance, number of times the mouse entered the center, and time in which the animal remained motionless, named freezing time, were registered by the

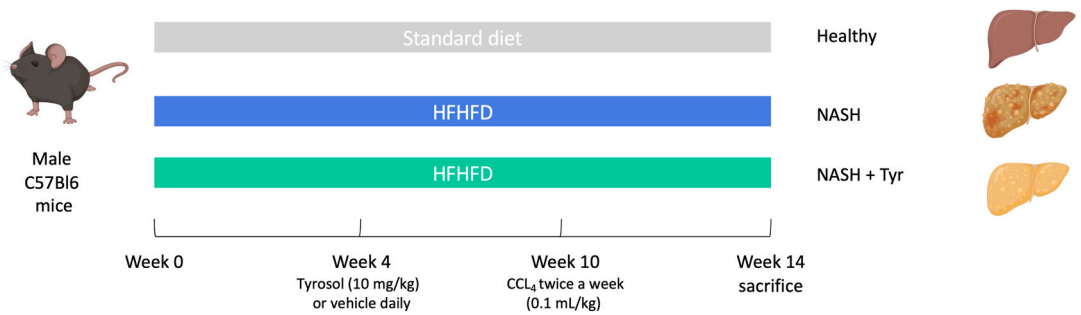

Fig. 1. Design of the *in vivo* study. Mice were randomly divided into the three experimental groups. HFHFD: high fat high fructose diet.

Anymaze software.

Forced Swim test: The Forced swim test was used to evaluate the depressive-like behavior of mice (Yankelevitch-Yahav et al., 2015). After 1 h of habituation, mice were placed in a transparent cylinder of 20 cm in diameter, filled with water at 23–25 °C, and its behavior was recorded for 6 min. For analysis purposes, only the last 4 min of recording were considered. Freezing time, reflecting the depressive-like state of the animal, was considered as the time in which the mouse floated without any movement except those necessary to keep the head out of the water. Also, the number of freezing episodes was registered.

2.9. Liver histology and immunohistochemistry of NOXs and Acta2

After fixation in formalin, the liver tissue was paraffin-embedded to perform histological analysis by means of the Masson trichrome, O Red Oil and H&E staining, using standard protocols. To analyze the protein expression of NOX1 and Acta2, immunohistochemical analyses were performed on 5-μm hepatic tissue sections, as previously described (De Martin et al., 2014). A heat-induced epitope retrieval was conducted for 20 min in citrate buffer (pH 6) for NOX1, and in Tris-EDTA buffer (pH 7.6) for Acta2. Slices were treated for 10 min with 0.2% Triton in PBS with Tween 20 (PBS-T), followed by a blocking step at RT with 5% FBS and 1% bovine albumin serum (BSA) in PBS-T. Liver sections were incubated overnight at 4 °C with primary antibodies anti-NOX1 or Acta2. Endogenous peroxidases were blocked by treating the sections for 20 min with 3% H_2O_2. Secondary antibodies were incubated for 1 h at 37 °C. Liver sections were then incubated with DAB and counterstained with hematoxylin, dehydrated and mounted with the EUKITT. Stained liver sections were examined by the same person, blinded to any information about the treatment. All the histological images were acquired with a Nikon Eclipse Ti–S microscope (10X or 20× magnification) and analyzed with the ImageJ software.

2.10. Flow cytometry

The portion of liver tissue placed in saline solution was processed to obtain a single-cell suspension for flow cytometry analysis, by the incubation for 1 h at 37 °C with a solution of 400 U/mL collagenase D (Sigma Aldrich, St. Luis, MO, USA) and 0.005 μg/mL DNAse to allow the enzymatic digestion of the tissue. The obtained cell suspension was filtered through a 100 μm-cell strainer, and cells were counted in Bucker chamber. A suspension of 1×10^6 cells/mL were incubated with the primary antibodies for 15 min at RT and fixed with PFA 4% (Diapath SPA, Bergamo, Italy). For the detection of the intracellular antigens, cells were permeabilized with 0.1% of Tween 20.1×10^6 cells/mL were incubated with anti-CD16/32 (2.4G2, BioXCell, Lebanon, NH, USA) for 15 min at room temperature to avoid unspecific binding of the antibodies. The antibodies used for flow cytometry analysis are reported in Table 1. These analyses were performed by means of a BD FACSAria™ III Cell Sorter (BD Bioscience, San Jose, CA, USA), and data were analyzed using the FlowJo v.10.0.8 software.

2.11. Quantification of gene expression in hepatic tissue

Total RNA was extracted from hepatic tissue as previously reported (Gabbia et al., 2020). One step qRT-PCR on extracted total mRNA was performed by means of CFX Opus 96 Real-Time PCR System (BioRad, CA, USA) using QuantiNova SYBR Green RT-PCR Kit (Qiagen, Hilden, Germania). Relative gene expression of the genes reported in Table 2 was calculated with the $2^{-\Delta\Delta Ct}$ method using β-actin as the housekeeping gene.

2.12. Statistical analyses

Statistical analyses were performed by one-way ANOVA and Kruskal–Wallis non-parametric analysis data using GraphPad Prism software ver. 9.0 (San Diego, CA, USA). $P < 0.05$ was considered statistically significant. If not otherwise stated, data are presented as mean ± standard error of the mean (S.E.M.).

Table 1
Specific antibodies used for cytometer analysis.

Antigen	Antibody	Dilution	Supplier
CD45	Alexa Fluor 700-conjugated anti-mouse CD45	1:200	eBioscience, Thermo Fisher Scientific, Waltham, MA, USA
F4/80	APC- conjugated anti-mouse F4/80	1:50	BioRad, CA, USA
CD86	Pe-Cy5-conjugated anti-mouse CD86	1:200	eBioscience, Thermo Fisher Scientific, Waltham, MA, USA
CD206	PE-conjugated anti-mouse CD206	1:200	eBioscience, Thermo Fisher Scientific, Waltham, MA, USA
CD3	PE-Cy7-conjugated anti-mouse CD3	1:200	BioLegend, San Diego, CA, USA
NKp46	BV421-conjugated anti-mouse NKp46	1:200	BioLegend, San Diego, CA, USA
PD1	PerCP-Cy5.5-conjugated anti-mouse CD279	1:200	BioLegend, San Diego, CA, USA
CD4	PerCP-Cy5.5-conjugated anti-mouse CD4	1:200	eBioscience, Thermo Fisher Scientific, Waltham, MA, USA
CD8	BV421-conjugated anti-mouse CD8a	1:125	BioLegend, San Diego, CA, USA
FOXP3	APC-conjugated anti-mouse FOXP3	1:125	eBioscience, Thermo Fisher Scientific, Waltham, MA, USA
CD62L	PE-conjugated anti-mouse CD62L	1:200	eBioscience, Thermo Fisher Scientific, Waltham, MA, USA

Table 2
Primers used for qRT-PCR analysis on liver tissues.

Target	Forward	Reverse
IL6	CCGGAGAGGAGACTTCACAG	TCCACGATTTCCCAGAGAAC
TGF-β1	GTGGAAATCAACGGGATCAGC	GTTGGTATCCAGGGCTCTCC
IL10	GCTGGACAACATACTGCTAACC	CTGGGGCATCACTTCTACCA
β-actin	ATGTGGATCAGCAAGCAGGA	AAGGGTGTAAAACGCAGCTCA

3. Results

3.1. Tyr attenuates lipid accumulation and oxidative stress in cellular models of steatosis

The effect of Tyr on lipid accumulation and the production of reactive oxidative species (ROS) was evaluated in a 2D model of steatosis set up by treating HepG2 cells with a FAs mixture in presence of increasing concentration of Tyr. As reported in Fig. 2, the treatment with FAs induced a significant increase of intracellular lipid droplets, that returned to the basal level after Tyr treatment that significantly decreased LD area inside the cells in a dose-dependent manner. Moreover, Tyr was able to significantly counteract the increase of ROS production caused by the FAs, that was similar to that induced by hydrogen peroxide, a typical cellular pro-oxidant stimulus (Fig. 2C).

Since cell–cell communication is a fundamental feature in the hepatic microenvironment and proinflammatory macrophages could sustain NASH-derived hepatic inflammation (Ghosh et al., 2023), we assessed Tyr effect on a co-culture of PA:OA-treated HepG2 and THP1-derived M1 macrophages. The reduction of lipid droplets induced by Tyr at the highest concentrations was maintained also in this more complex experimental setting (Fig. 3).

3.2. Tyr decreases lipid accumulation and CD86 expression in multicellular spheroids

In order to confirm the effect of Tyr on reducing lipid accumulation in a more complex model in vitro, we set up a MCSs by co-seeding HepG2 and LX2 and, subsequently adding THP1-derived MΦ

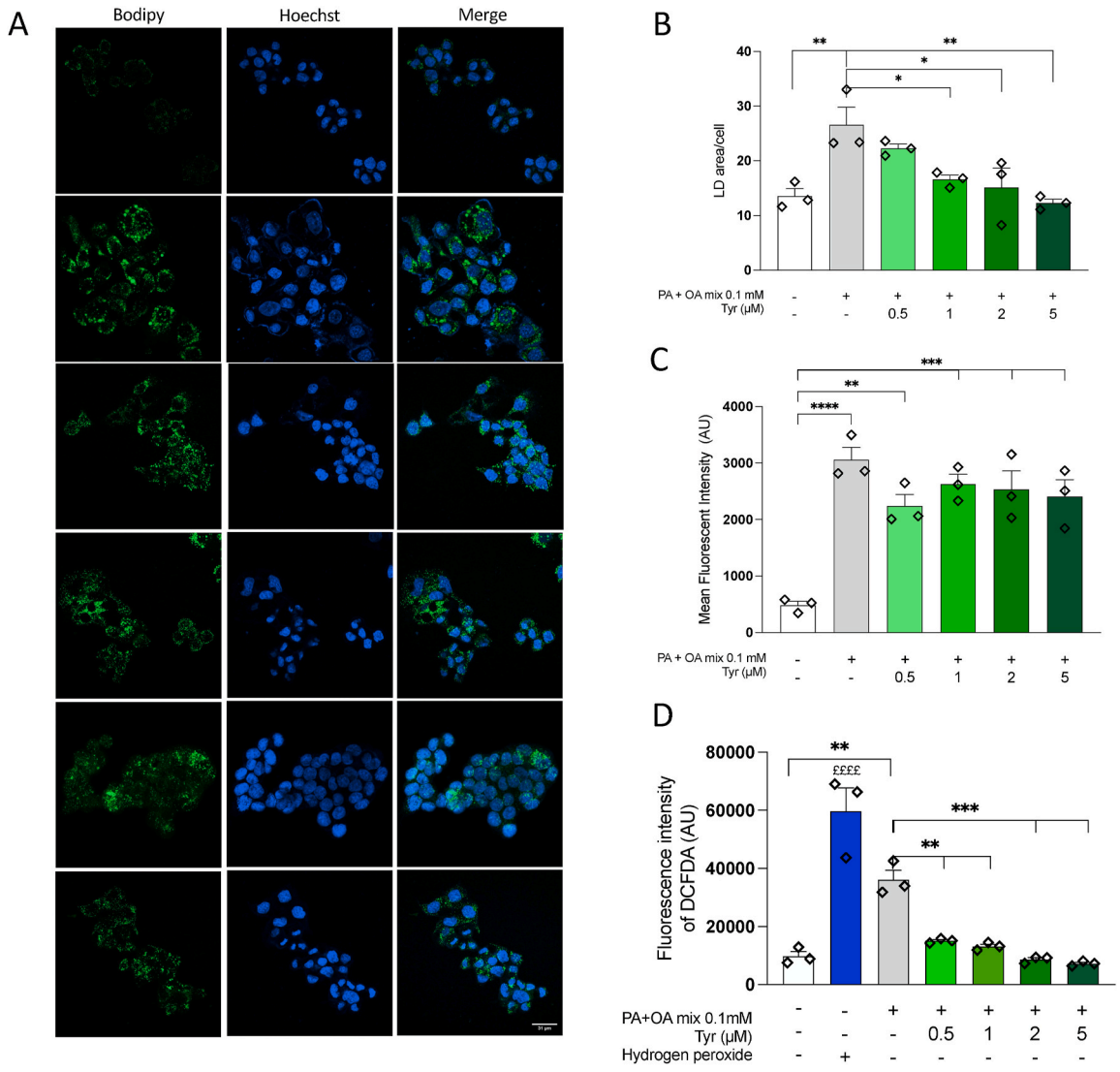

Fig. 2. *In vitro* effect of Tyr on the formation of lipid droplets (LDs) in HepG2 cells treated with the PA:OA mixture. LDs are stained green with Bodipy and nuclei stained blue with Hoechst (A). The quantification of LDs is reported as LD area/cell (B) and Bodipy mean fluorescence intensity (C). Effect of Tyr on ROS production by HepG2 cells assessed by means of DCFDA assay and reported in the graph as DCFDA mean fluorescence intensity (D). Data are reported as mean ± S.E.M. of three different experiments, each done in triplicate. *$p < 0.05$, **$p < 0.01$, and ***$p < 0.001$. $^{\text{£££}}p < 0.0001$ vs. all the other conditions.

macrophages and treating with the PA:OA mix. Nor the PA:OA mix or Tyr treatment had effect on spheroid vitality, sphericity index and spheroid volume as reported in Fig. S1, thus confirming the absence of detrimental effects on cell viability. As expected, the PA:OA mix significantly increased lipid accumulation, as assessed by the Nile red stain. Tyr treatment reduced this accumulation and restored physiological condition at the two concentrations used in this assay (Fig. 4A–C). Moreover, the increased lipid accumulation in the MCSs was accompanied by an increase of CD86 expression, indicating the differentiation of MΦ macrophages toward a pro-inflammatory M1 phenotype, without effects on the capacity of macrophages of infiltrating the spheroids, as demonstrated by the lack of changes of CD68 expression (Fig. 4D and E). This effect was completely prevented by Tyr treatment, that avoided this pro-inflammatory switch (Fig. 4D–F).

3.3. Tyr decreases fibrogenesis in multicellular spheroids

To assess the effect of Tyr on fibrogenesis in a lipid overload condition, resembling the two key features of NASH, namely fibrosis and steatosis, we added to the above described MCS the prototypical fibrogenic stimulus TGF-β1. In this model, we observed an increased protein expression of the profibrogenic Acta2, marker of LX-2 activation, induced by the treatment with PA:OA mix with respect control cells (Fig. 5). As expected, this increase was more evident when the PA:OA mix was used in combination with TGF-β1, suggesting that this two stimuli, typically present in the NAFLD/NASH transition, prompt LX-2 activation. Tyr was able to revert significantly this increase at both concentrations. In particular, the highest concentration restored the basal level of Acta2 expression, suggesting that Tyr might exert an antifibrotic effect in a NASH setting.

3.4. Tyr improves hepatic steatosis and fibrosis in a NASH in vivo model, and reduces inflammation by affecting hepatic immune cell phenotypes

To corroborate our in vitro results, we studied the effect of Tyr on all the pathological features of NASH, namely steatosis, fibrosis and inflammation, in a mouse model of NASH (Zhang et al., 2020).

NASH animals displayed a significant increase of lipids and of hypertrophic hepatocytes with respect to healthy animals, as assessed by the ORO staining (Fig. 6). This increase was effectively counteracted by Tyr treatment, that decreased the percentage of steatotic areas and hypertrophic hepatocytes. No effect was observed in hepatic TG content,

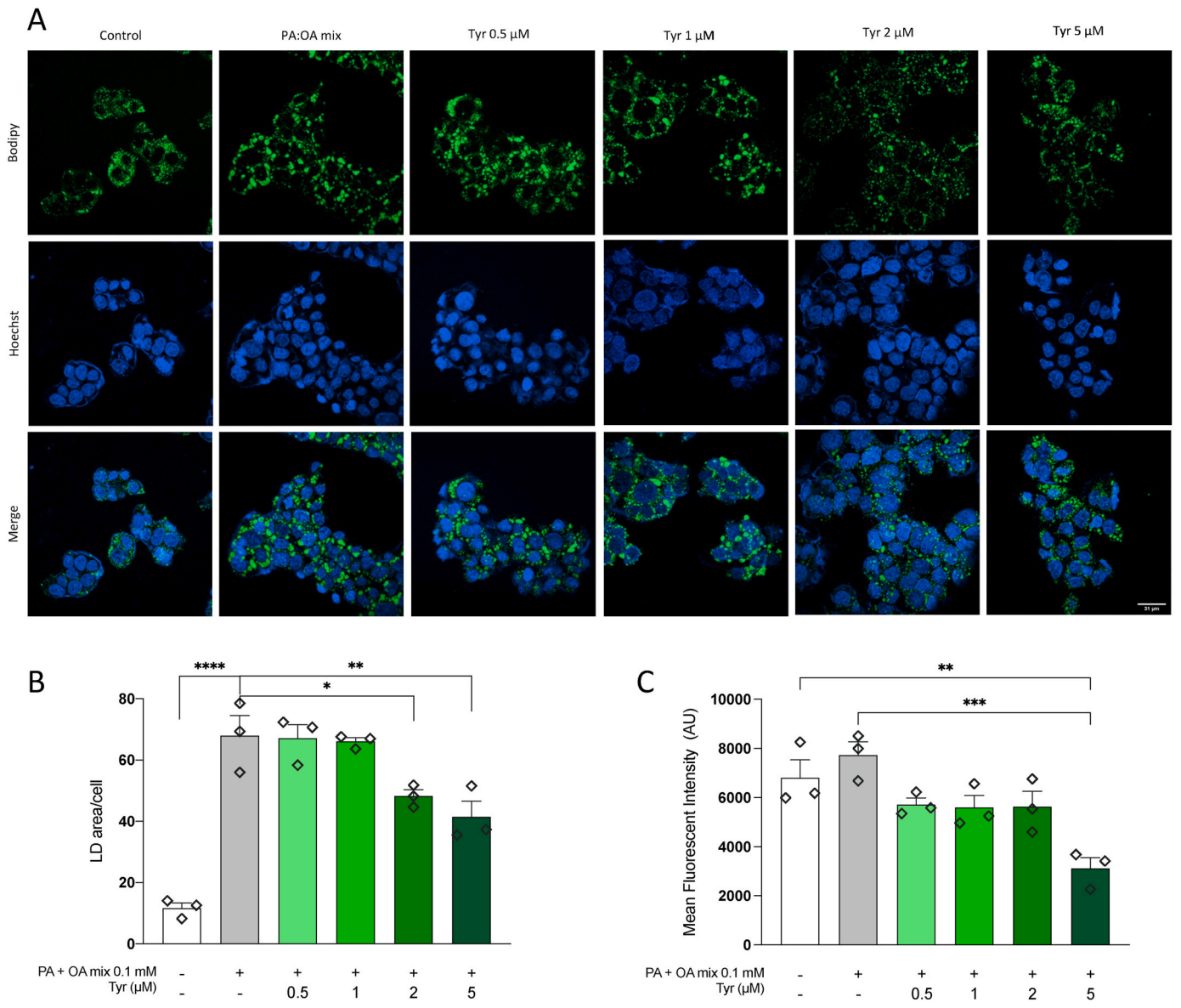

Fig. 3. *In vitro* effect of Tyr on the formation of LDs in a co-culture of HepG2 cells and M1-macrophages. LDs are stained green with Bodipy and nuclei stained blue with Hoechst (A). The quantification of LDs is reported as LD area/cell (B) and Bodipy mean fluorescence intensity (C). Data are reported as mean ± S.E.M. of three different experiments, each done in triplicate. *p < 0.05, **p < 0.01, ****p < 0.0001.

even though an increasing tendency to higher level in NASH animals could be appreciated.

As reported in Fig. 7, HFHFD induced a significant deposition of fibrotic tissue, and coherently a significant increase of Acta2 protein expression, marker of HSC activation. Tyr was able to reduce fibrotic areas and Acta2 expression, restoring basal levels. Accordingly, Tyr treatment counteracted the upregulation of TGF-β1 mRNA expression observed in NASH mice (Fig. 7G). Moreover, the increasing tendency of the prooxidant enzyme NOX1 observed in NASH animals seems to be reduced by Tyr treatment, even though not at statistically significant level (Fig. 7E and F). Taken together, these results demonstrated that Tyr positively affected NASH-related inflammation and fibrogenesis, by reducing TGF-β1 transcription in hepatocytes, Acta2 expression in HSCs, and modulating NOX1 expression.

Due to the importance of inflammatory processes in the different stages of MASLD (Gabbia et al., 2019), and the lack of knowledge on Tyr effect on immune modulation, we performed a detailed analysis of the immune cells present in the liver in our model. As reported in Fig. 8, the significant increase of inflammatory foci in hepatic parenchyma observed in NASH mice was effectively counteracted by Tyr. This preliminary histological finding was in line with flow cytometry results. First, as observed in vitro, we demonstrated that the increase of hepatic pro-inflammatory $CD86^+$ macrophages observed in NASH mice was reduced by Tyr also *in vivo*, returning to basal levels, thereby confirming its inhibition on the M1 phenotype. This effect was accompanied by a marked reduction of IL6 mRNA expression in the hepatic tissue (Fig. 8F). Adoptive immune cells were also affected. In fact, NASH animals displayed an increase of total $CD4^+$ $CD8^-$ T cells as well as $T_{helper\ effector}$ $CD4^+$ $FoxP3^+$ $CD62L^-$ cells with respect to healthy mice (Fig. 8D), that was effectively reduced by Tyr treatment. Notably, Tyr was able to also increase the number of T_{reg} cells, with respect to the other two groups (Fig. 8E). This result, together with the increase of IL-10 mRNA expression suggested Tyr involvement in the activation of regenerative pathways, in which Tregs play a pivotal role (Wu et al., 2023).

3.5. Tyr prevents NASH-related extrahepatic manifestations

Recently, attention has been raised to the extrahepatic

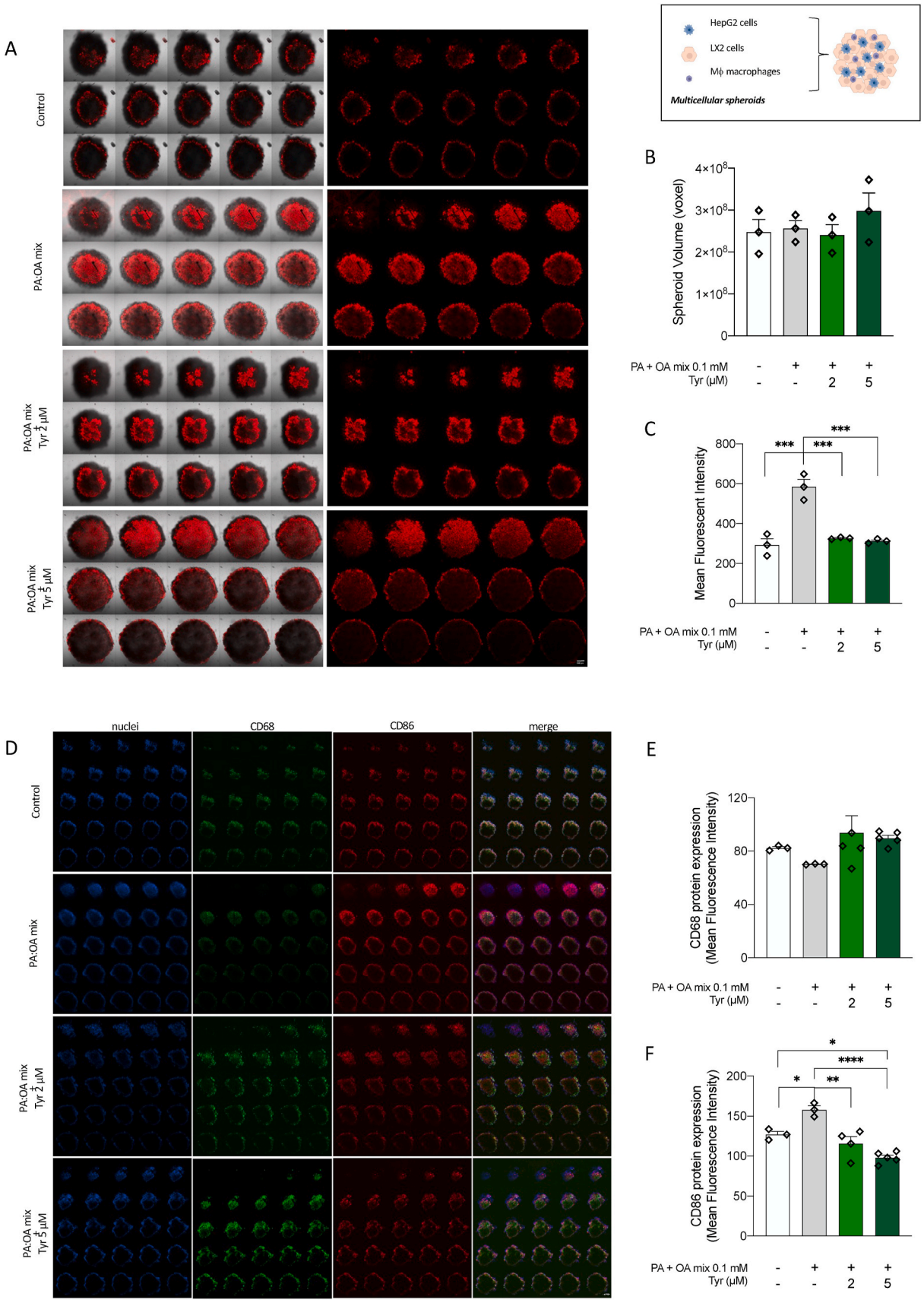

Fig. 4. *In vitro* effect of Tyr on the MCS model. Confocal images of lipid droplets (in red) obtained by Nile red stain (A) and analysis of spheroid volume (B) and red fluorescence intensity (C). Confocal images of MCSs stained with Hoechst (nuclei), anti-CD68 (green) and anti-CD86 (red) in (D) and relative quantification of CD68 (E) and CD86 (F) reported as AU of fluorescence intensity. Data are reported as mean ± S.E.M. of three different experiments, each done in triplicate. *$p < 0.05$, **$p < 0.01$, ***$p < 0.001$, ****$p < 0.001$.

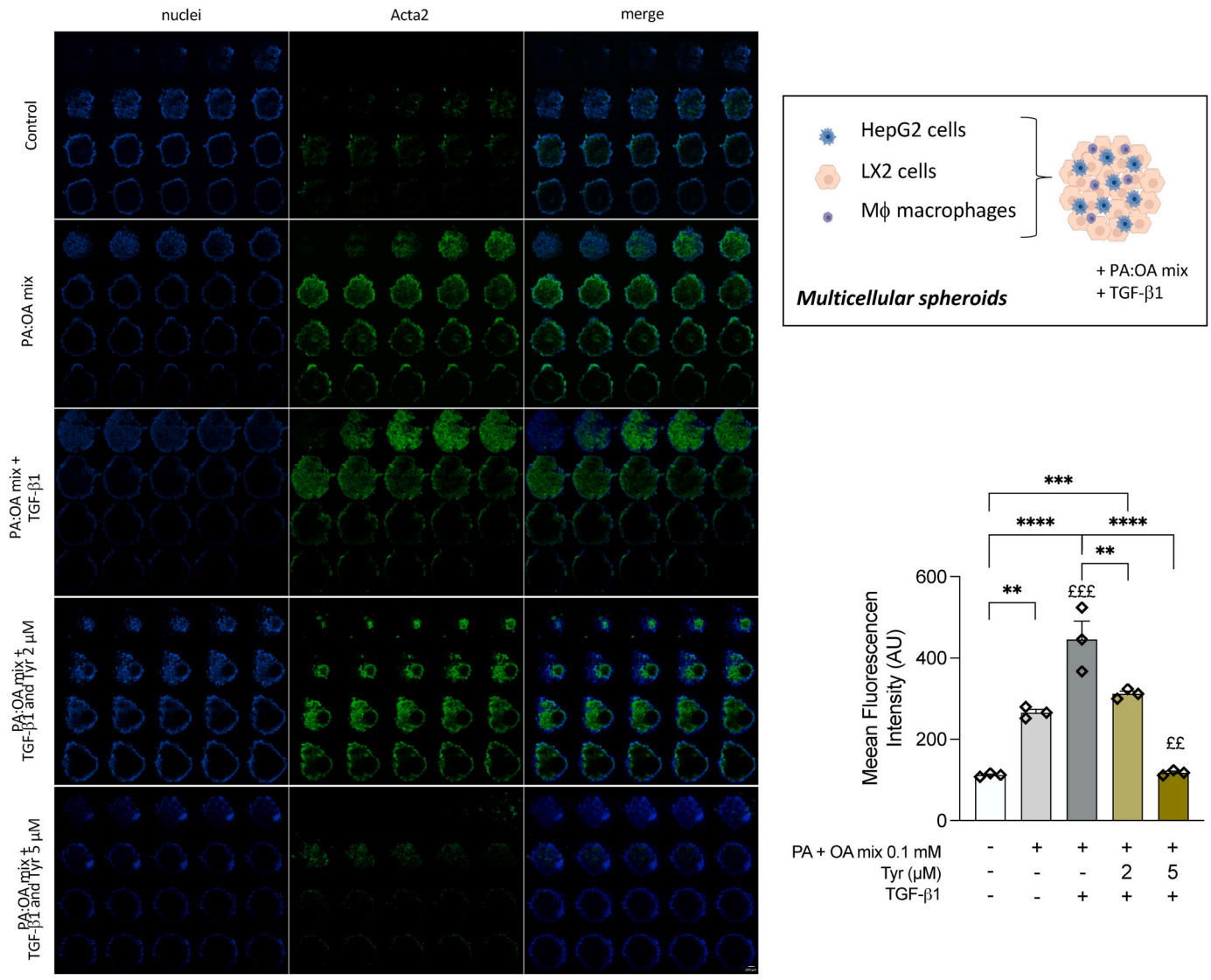

Fig. 5. *In vitro* effect of Tyr on MSCs set up by seeding HepG2 and LX2 cells (1:1) and adding THP1-derived Mφ macrophages. PA:OA mix and TGF-β1 were used to increase lipid accumulation and LX-2 activation. LX-2 activation was measured as Acta2 protein expression increase, reported as mean fluorescence intensity (AU). Data are reported as mean ± S.E.M. of three different experiments, each done in triplicate. **p < 0.01, ***p < 0.001, ****p < 0.0001. $^{££}$p < 0.01 and $^{£££}$p < 0.001 vs PA:OA mix-treated cells.

manifestations of NAFLD/NASH, including for example cognitive impairment and depression (Colognesi et al., 2020), that may further worsen NASH patients' quality of life of. To this purpose, several methods have been developed to assess the degree of the so called health-related quality of life (HRQL) in NASH patients measuring some parameters informative of their general health e.g. physical, emotional, mental, and social well-being (Stepanova et al., 2023). In this study, we assessed these aspects by means of a panel of behavioral studies, investigating the effect or Tyr on motor dysfunction, depressive-like behavior, and anxiety status.

Motor function was evaluated by means of grid (A), gripping (B) and rotarod (C) tests, measuring both muscle strength and coordination (Fig. 9). In these tests, we observed a significant decrease of muscular strength and coordination in NASH mice, as outlined by the rotarod (less time spent on the rod) and gripping test, respectively. These decreases of physical performance were restored by Tyr (Fig. 9B and C).

Tyr treatment also induced an improvement of central nervous system (CNS) symptoms, by reducing depressive-like behavior (number of freezing episodes) in the Forced Swim test (Fig. 9D), and anxious behavior (freezing time) in the Open Field test (Fig. 9E). Taken together, these data suggested that, beside or because of its peculiar hepatic effect on NASH, Tyr also improves the general health status of this mouse model of NASH.

4. Discussion

The prevalence of MASLD has dramatically raised in the last decade, together with its comorbidities, e.g. obesity, insulin resistance and type 2 diabetes. A further increase is expected in the next years (Hamid et al., 2022), since current projections estimate that more than 300 million people in China, 15–20 million in Europe and more than 100 million in the USA will develop NAFLD by 2030 (Estes et al., 2018). NASH may develop as a complication of simple steatosis and is characterized by the simultaneous presence of steatosis, inflammation, and fibrosis. Among MASLD patients with an indication for biopsy, about 60–70% have biopsy-proven NASH, and among those patients without an indication for biopsy, this percentage is variable from 6.67% in Asia to 29.85% in North America (Younossi et al., 2017). Since NASH can progress towards cirrhosis and/or HCC, it has been estimated that patients with NASH-related HCC will increase in next years. This scenario collocates

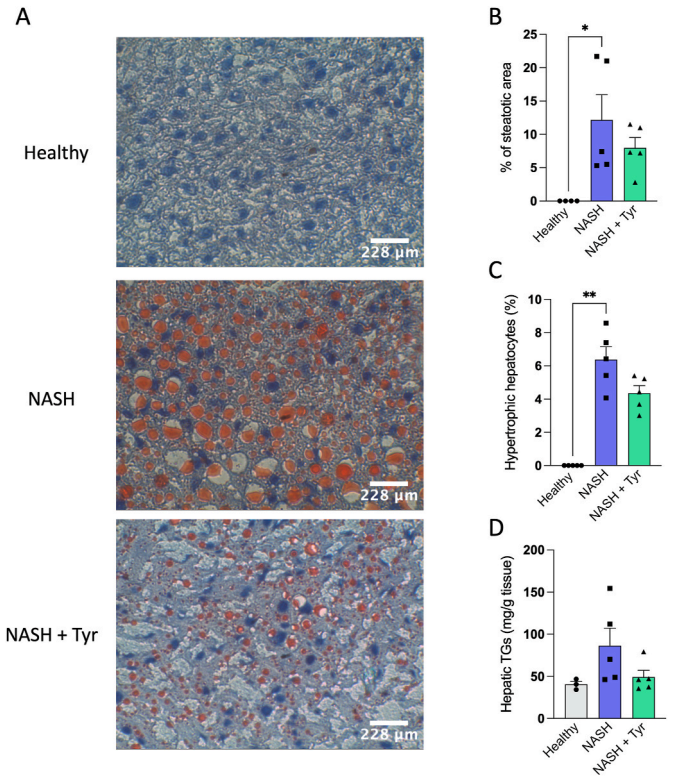

Fig. 6. *In vivo* effect of Tyr on liver steatosis. Histological images, 20× magnification (A), quantification of steatotic areas (B), steatotic hepatocytes (C) and hepatic TG content (D). Data are reported as mean ± S.E.M. (n = 5 animals per group) *p < 0.05, **p < 0.01.

NASH treatment as a major clinical challenge for hepatologists and the scientific community worldwide. The onset of MASLD is driven by the dysregulation of three main mechanisms occurring in hepatocytes, i.e., the accumulation of fatty acids (FAs) due to their increased uptake, the increase of *de novo* lipogenesis and cholesterol accumulation in endoplasmic reticulum (ER), and the decrease in the mitochondrial oxidation of FAs (Berlanga et al., 2014). Targeting these mechanisms may be exploited as a strategy to prevent or slow down the multiple stressors involved in NASH development. This study aimed at assessing the efficacy of Tyr in improving the three hallmarks of NASH, i.e., steatosis, fibrosis, and inflammation. We have previously demonstrated that Tyr is able to counteract hepatic fibrosis by the transcriptional modulation of the NADPH oxidases NOX1 and NOX4 and of the oxidative stress-related miRNAs miR-181–5p and miR-29b-3p (Gabbia et al., 2023) in models of liver fibrosis. Moreover, hydroxytyrosol, another phenolic compound of EVOO, has been recently proposed for MASLD treatment, due to its ability to alleviate steatosis, oxidative stress, inflammation and mitochondrial dysfunction (Dong et al., 2022; Echeverría et al., 2022; Gori et al., 2021; Pirozzi et al., 2016). In addition, a novel combination of hydroxytyrosol and vitamin E has been recently tested in pediatric patients with steatosis with positive results, since the reduction of hypertriglyceridemia and systemic inflammation, and an increase of circulating IL-10 was observed in this patients after treatment (Mosca et al., 2021).

The persistent presence of cellular FAs and reactive oxygen species (ROS) leads to lipotoxicity, ER stress, mitochondrial damage and oxidative stress (Huby and Gautier, 2022) and these multiple cellular stressors lead to NASH onset (Huby and Gautier, 2022). In this study, we first demonstrated that Tyr treatment was able to reduce the accumulation of FAs inside hepatocytes and reduce ROS production in different in vitro 2D models of NAFLD and NASH.

To assess the effect on Tyr on a more complex cellular model mimicking the three main features of NASH, namely inflammation, fibrosis, and steatosis, we set up MCSs using three cell lines resembling the main cells of the hepatic microenvironment, i.e., HepG2 cells (hepatocytes), LX-2 cells (hepatic stellate cells) and THP-1 cells (Kupffer cells or macrophages). Also in this model, Tyr treatment was effective in reducing the accumulation of FAs and concurrently reduced the expression of CD86 in macrophages, suggesting its ability to affect their polarization to an anti-inflammatory phenotype. Furthermore, we confirmed the anti-fibrotic effect of Tyr also in this complex in vitro model, since Tyr effectively reduced Acta2 expression, thereby indicating the reduction of LX-2 activation, even in the excess of FAs.

The effect of Tyr was also assessed *in vivo* in a murine model of NASH, obtained by feeding mice for 14 weeks with a high-fat high-fructose diet and the injection of low doses of the hepatotoxic agents CCl_4. The antifibrotic effect of Tyr was confirmed also in this setting, since we observed a reduced activation of HSC, as indicated by a decrease of TGF-β1 transcription and Acta2 expression in the hepatic tissue of NASH animals. Tyr also led to a reduction of steatotic areas and of the number of hypertrophic hepatocytes and this effect was accompanied by a reduction of inflammation, since a decrease of IL6 upregulation and a reduction of the inflammatory foci in the hepatic parenchyma could be observed. IL6 is a typical pro-inflammatory chemokine that sustains the exacerbation of MASLD in the hepatic parenchyma and may also be implicated in the progression towards a tumoral transition (Chan et al., 2019; Xi et al., 2021). It has been demonstrated that huge intake of fructose is responsible for the increase of hepatic de novo lipogenesis and intestinal permeability, that prompts the activation of hepatic immune cells by TLR-dependent pathway modulated by gut-derived inflammatory mediators (Todoric et al., 2020). Moreover, this dysbiosis-related increased permeability further sustains hepatic inflammation and sensitizes hepatocyte to cell death. These processes lead to the release of pro-inflammatory mediators, such as for example IL6, inducing the activation of HSCs and fibrogenesis. All together, these events represent an vicious self-feeding cycle whose exacerbation leads to cirrhosis and HCC development (Huby and Gautier, 2022). Thus, increased IL6 release may exacerbate NASH and liver fibrosis (Xiao et al., 2023). IL6 is also implicated in senescence-associated necroptosis, a cell death pathway that induces inflammation through the release of damage-associated molecular patterns (DAMPs), endogenous danger signals that are increased in NASH (Mihm, 2018). A necroptosis inhibitor has demonstrated to reduce pro-inflammatory M1-like macrophages and improve inflammation in aged mice (Mohammed et al., 2021). We demonstrated that also Tyr reduced the hepatic accumulation of $CD86^+$ macrophages, confirming our in vitro data and suggesting Tyr ability to modulate hepatic innate immune macrophagic population towards an anti-inflammatory status. In the liver, macrophages crosstalk with HSCs through several molecular mechanisms, e.g. M1 macrophages can promote their activation by releasing TGF-β1 and other profibrogenetic cytokines (Alisi et al., 2017). Proinflammatory M1-like macrophages, also termed “classically activated”, produce proinflammatory cytokines, e.g. IL-6, IL-1β, IL-8, IL-12, and TNF-α, thus triggering injury of the hepatic tissue (Sica et al., 2014). In our NASH model, the reduction of IL6 overexpression observed in Tyr-treated mice was also accompanied by the downregulation of NOX1 and TGF-β1 and expression, thus suggesting that Tyr may reduce ROS overproduction due to NOX upregulation, and modulate the crosstalk between proinflammatory macrophages and HSCs, preventing their activation and thus fibrosis. Taking all these observations together, we demonstrated that Tyr improves steatosis, inflammation, and fibrosis in different NASH models.

A large spectrum of different immune cell subsets patrols the hepatic parenchyma, such as natural killer (NK) cells, $CD4^+$ and $CD8^+$ T cells, both resident and temporarily recruited from circulation (Huby and Gautier, 2022). These immune cells establish complex connections with HSC and hepatocytes, reciprocally influencing their activation and activity, and this complex scenario may be altered in chronic liver disease. In NASH, an accumulation of $CD4^+$ T cells in hepatic parenchyma has

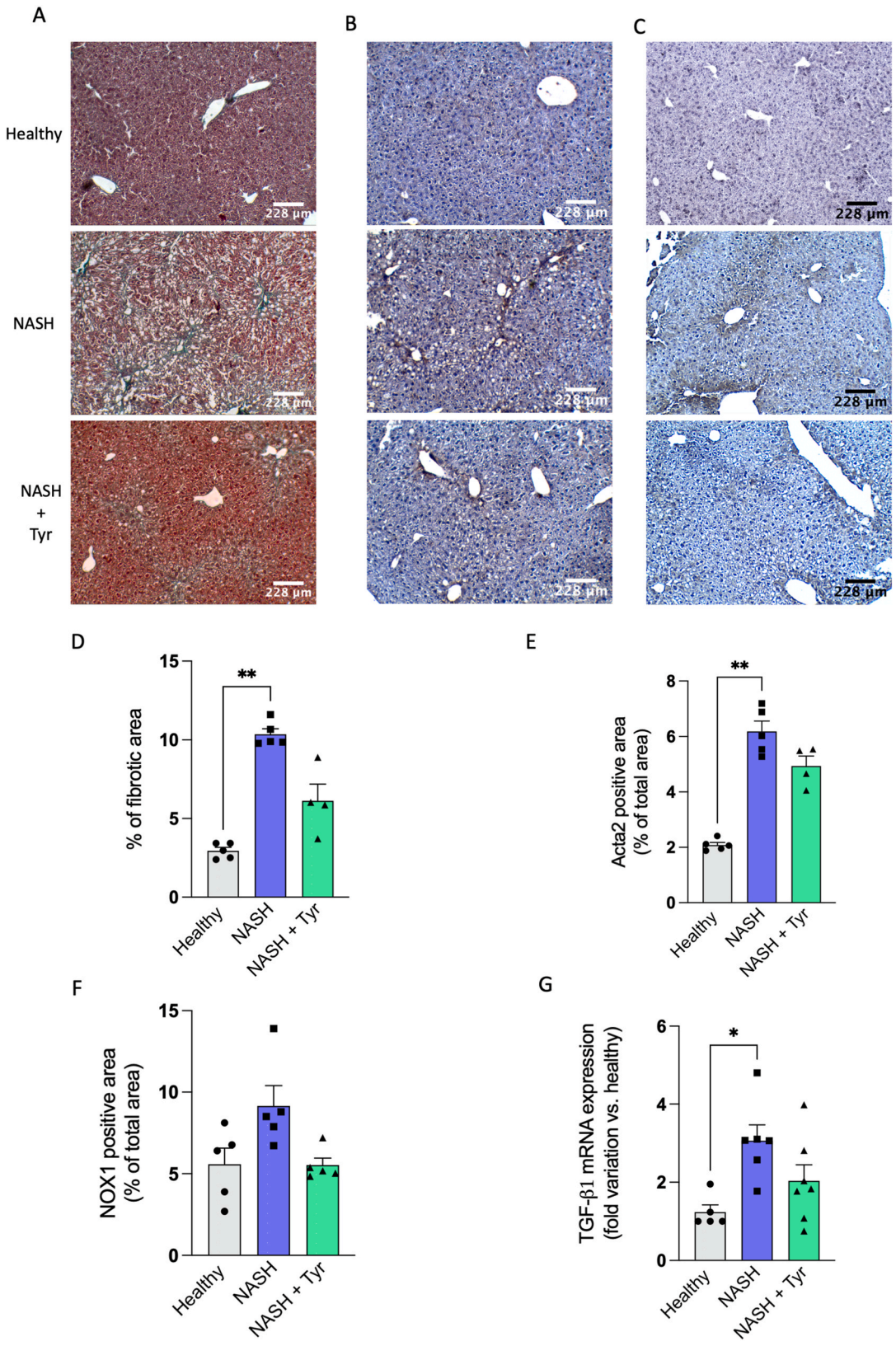

Fig. 7. In vivo effect of Tyr on hepatic fibrosis. Histological images, 10× magnification (A) and quantification of the fibrotic areas (D). Acta2 protein expression in hepatic tissue; immunohistochemical microphotographs (10× magnification, B) and quantification (E). NOX1 protein expression; immunohistochemical microphotographs (10× magnification, C) and quantification (F). TGF-β1 mRNA expression (G). Data are reported as mean ± S.E.M (n = 5 animals per group). *$p < 0.05$, **$p < 0.01$.

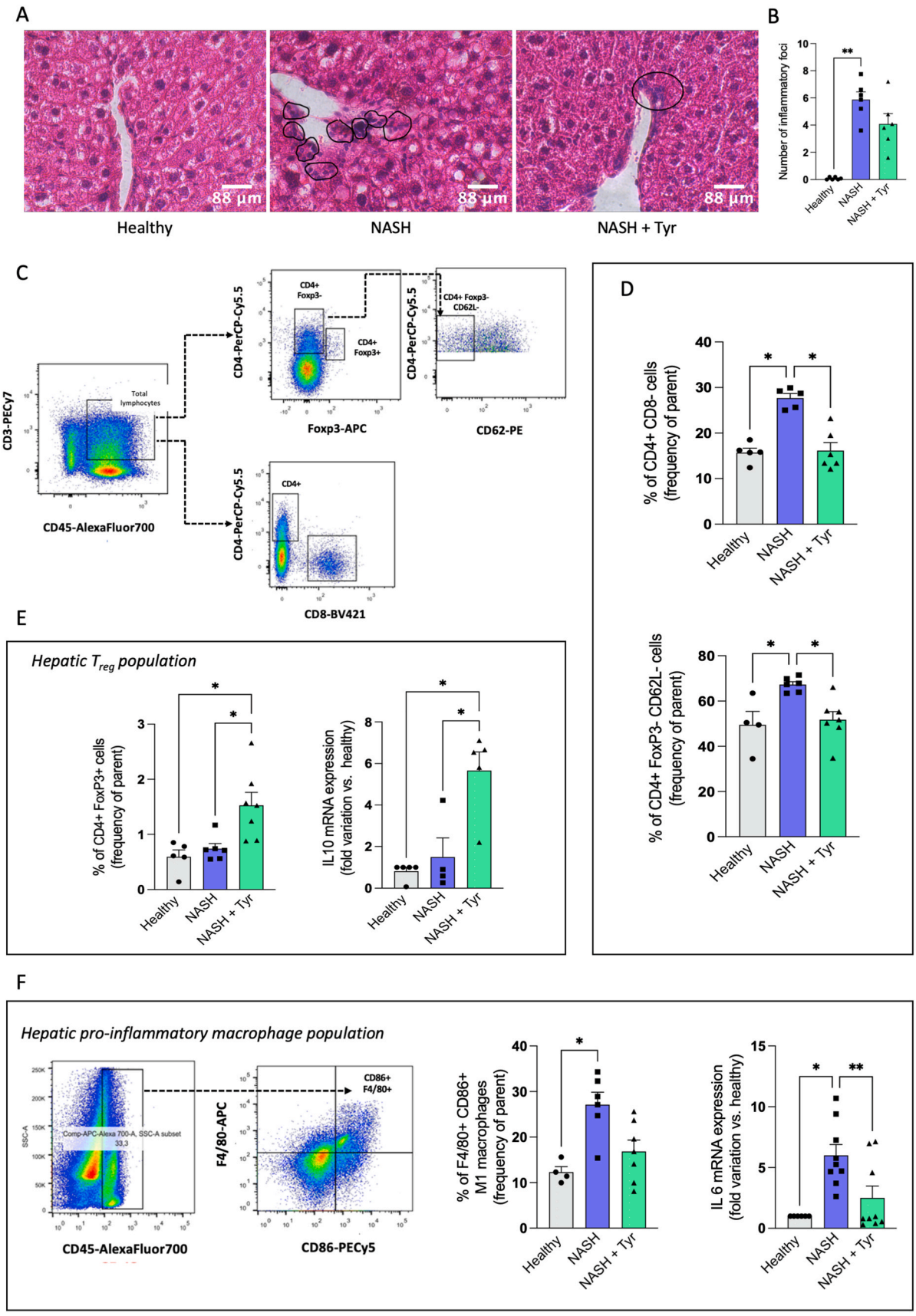

Fig. 8. *In vivo* effect of Tyr on inflammation. Number of inflammatory foci (A, round circles, and their quantification, B); pro-inflammatory M1 macrophages (C, gating strategy shown as pseudo-color plot of FACS analysis and quantification, and IL6 mRNA expression in hepatic tissue); $CD4^+$ T cell subsets (D, gating strategy shown as pseudo-color plot of FACS analysis); hepatic T_{reg} $CD4^+$ $FoxP3^+$ cells and IL10 mRNA expression (E); hepatic $CD4^+$ $CD8^-$ T lymphocytes and $T_{helper\ effector}$ $CD4^+$ $FoxP3^+$ $CD62L^-$ cells (F). Data are reported as mean ± S.E.M. (n = 5 animals per group). *p < 0.05, **p < 0.01.

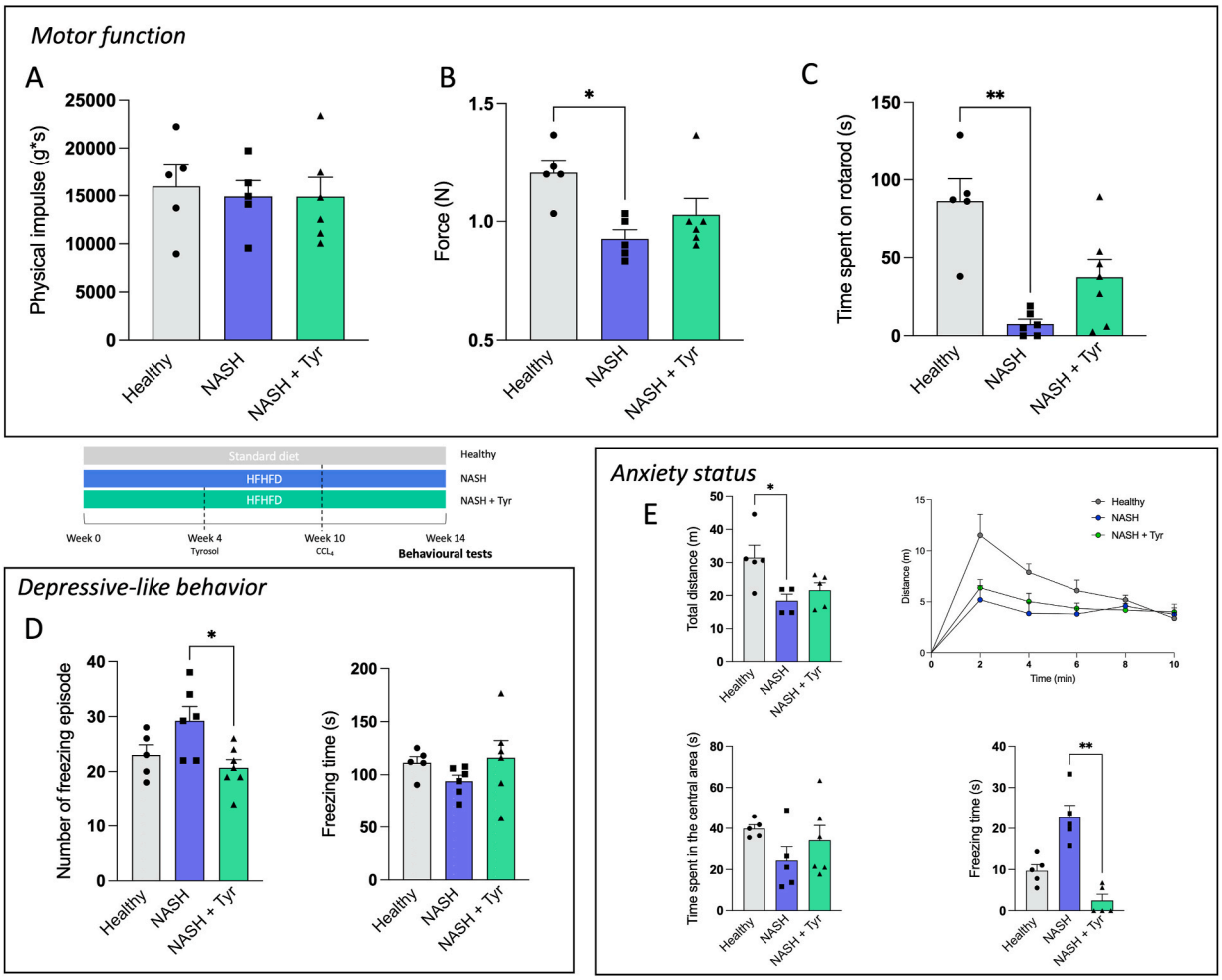

Fig. 9. Tyr effect on the extrahepatic manifestations of NASH. Motor function, assessed by grid (physical impulse, A), gripping (force, B) and rotarod (time spent on the Rod, C) tests. CNS symptoms assessed by Forced swim (number of freezing episodes and freezing time, D) and Open Field (total distance, time spent in the central area, freezing time, E) tests. Data are reported as mean ± S.E.M. (n = 5 animals per group). *p < 0.05, **p < 0.01.

been observed both in human and murine models (Sutti and Albano, 2020; Zhou et al., 2022), suggesting a fundamental role of adaptive immunity in driving MASLD progression. Notably, in the present study we observed that the increase of the $CD4^+$ $CD8^-$ T cells observed in NASH liver was restored to basal levels after Tyr treatment. Interestingly, we observed that Tyr treatment effectively increased Treg population, that has been involved in the promotion of regenerative pathways (Kisseleva and Brenner, 2021), thus suggesting that Tyr may play an active role also in liver regeneration. It worth noticing that recent evidence reported a contradictory role for Treg in fibrosis, since they can either inhibit or promote HSC activation. However, the promotion of fibrosis relies on the conversion of Tregs into cells expressing IL17, which occurs in the presence of IL6 (Wu et al., 2023), whereas the inhibition of fibrosis is mainly due to IL10-induced pathways. Therefore, the Tyr-induced IL6 decrease and IL10 increase shed a new light on its possible antifibrotic mechanism, suggesting the pivotal involvement of Tregs. Further studies are needed to unravel the role of Tyr in this context.

Beside the hepatic symptoms, NASH could induce extrahepatic manifestations, e.g. cognitive impairment, depression and motorial dysfunction, that may lead to a great impairment of the patients' quality of life (Colognesi et al., 2020; Stepanova et al., 2023). To assess whether Tyr-induced amelioration of the hepatic condition could also affect extrahepatic NASH-related issues, we performed a panel of behavioral tests to assess the effect of Tyr on general health status of NASH mice, demonstrating its usefulness in improving the muscular strength and coordination impairment observed in NASH animals and also their depressive-like and anxious behavior.

In conclusion, according to our knowledge, this is the first report demonstrating that Tyr improves steatosis, fibrosis, and inflammation in NASH, exerting a modulatory activity on the hepatic immune milieu, by acting on cells responsible for both innate and adaptive immunity.

CRediT authorship contribution statement

Daniela Gabbia: Writing – review & editing, Writing – original draft, Project administration, Methodology, Investigation, Data curation, Conceptualization. **Katia Sayaf:** Investigation. **Ilaria Zanotto:** Investigation. **Martina Colognesi:** Investigation. **Yahima Frion-Herrera:** Investigation. **Maria Carrara:** Supervision. **Francesco Paolo Russo:** Supervision. **Sara De Martin:** Writing – review & editing, Supervision, Project administration, Methodology, Funding acquisition, Data curation, Conceptualization.

Declaration of competing interest

None.

Data availability

Data will be made available on request.

Acknowledgments

This research was supported by the University of Padova, grant code DEMA_SID19_01 (to SDM) and by the Italian Ministry of University and Research (MUR), grant PON 2014–2020 "Research and Innovation" resources—Green/Innovation Action—DM MUR 1062/2021—for the research EPAGREEN" (to SDM). The authors would like to thank Sara Campagnaro, Mauro Berto and Federico Cusinato for their skilled technical assistance.

Appendix A. Supplementary data

Supplementary data to this article can be found online at https://doi.org/10.1016/j.ejphar.2024.176453.

References

Alisi, A., Carpino, G., Oliveira, F.L., Panera, N., Nobili, V., Gaudio, E., 2017. The role of tissue macrophage-mediated inflammation on NAFLD pathogenesis and its clinical implications. Mediat. Inflamm. 2017, e8162421 https://doi.org/10.1155/2017/8162421.

Berlanga, A., Guiu-Jurado, E., Porras, J.A., Auguet, T., 2014. Molecular pathways in non-alcoholic fatty liver disease. Clin. Exp. Gastroenterol. 7, 221–239. https://doi.org/10.2147/CEG.S62831.

Chalasani, N., Younossi, Z., Lavine, J.E., Charlton, M., Cusi, K., Rinella, M., Harrison, S. A., Brunt, E.M., Sanyal, A.J., 2018. The diagnosis and management of nonalcoholic fatty liver disease: practice guidance from the American Association for the Study of Liver Diseases. Hepatology 67, 328–357. https://doi.org/10.1002/hep.29367.

Chan, L.-C., Li, C.-W., Xia, W., Hsu, J.-M., Lee, H.-H., Cha, J.-H., Wang, H.-L., Yang, W.-H., Yen, E.-Y., Chang, W.-C., Zha, Z., Lim, S.-O., Lai, Y.-J., Liu, C., Liu, J., Dong, Q., Yang, Y., Sun, L., Wei, Y., Nie, L., Hsu, J.L., Li, H., Ye, Q., Hassan, M.M., Amin, H.M., Kaseb, A.O., Lin, X., Wang, S.-C., Hung, M.-C., 2019. IL-6/JAK1 pathway drives PD-L1 Y112 phosphorylation to promote cancer immune evasion. J. Clin. Invest. 129, 3324–3338. https://doi.org/10.1172/JCI126022.

Colognesi, M., Gabbia, D., De Martin, S., 2020. Depression and cognitive impairment-extrahepatic manifestations of NAFLD and NASH. Biomedicines 8. https://doi.org/10.3390/biomedicines8070229.

Cui, J., Guo, T., Chao, J., Wang, M., Wang, J., 2016. Potential of the endophytic fungus phialocephala fortinii Rac 56 found in Rhodiola plants to produce salidroside and p-tyrosol. Molecules 21, 502. https://doi.org/10.3390/molecules21040502.

De Martin, S., Paliuri, G., Belloni, A., Orso, G., Zanarella, E., Stellin, G., Milanesi, O., Basso, G., Ruga, E.M., Frasson, C., Gabbia, D., Perdoncin, G., Palatini, P., Bova, S., 2014. Expression and distribution of the adrenomedullin system in newborn human thymus. PLoS One 9, e97592. https://doi.org/10.1371/journal.pone.0097592.

Deacon, R.M.J., 2013. Measuring the strength of mice. J. Vis. Exp. 2610 https://doi.org/10.3791/2610.

Dong, Q., Bao, H., Wang, J., Shi, W., Zou, X., Sheng, J., Gao, J., Guan, C., Xia, H., Li, J., Kang, P., Xu, Y., Cui, Y., Zhong, X., 2023. Liver fibrosis and MAFLD: the exploration of multi-drug combination therapy strategies. Front. Med. 10, 1120621 https://doi.org/10.3389/fmed.2023.1120621.

Dong, Y., Yu, M., Wu, Y., Xia, T., Wang, L., Song, K., Zhang, C., Lu, K., Rahimnejad, S., 2022. Hydroxytyrosol promotes the mitochondrial function through activating mitophagy. Antioxidants 11, 893. https://doi.org/10.3390/antiox11050893.

Echeverría, F., Bustamante, A., Sambra, V., Álvarez, D., Videla, L., Valenzuela, R., 2022. Beneficial effects of dietary polyphenols in the prevention and treatment of NAFLD: cell-signaling pathways underlying health effects. Curr. Med. Chem. 29, 299–328. https://doi.org/10.2174/0929867328666210825111350.

Estes, C., Razavi, H., Loomba, R., Younossi, Z., Sanyal, A.J., 2018. Modeling the epidemic of nonalcoholic fatty liver disease demonstrates an exponential increase in burden of disease. Hepatology 67, 123–133. https://doi.org/10.1002/hep.29466.

Frión-Herrera, Y., Gabbia, D., Cuesta-Rubio, O., De Martin, S., Carrara, M., 2019. Nemorosone inhibits the proliferation and migration of hepatocellular carcinoma cells. Life Sci. 235, 116817 https://doi.org/10.1016/j.lfs.2019.116817.

Frión-Herrera, Y., Gabbia, D., Scaffidi, M., Zagni, L., Cuesta-Rubio, O., De Martin, S., Carrara, M., 2020a. Cuban Brown propolis interferes in the crosstalk between colorectal cancer cells and M2 macrophages. Nutrients 12, 2040. https://doi.org/10.3390/nu12072040.

Frión-Herrera, Y., Gabbia, D., Scaffidi, M., Zagni, L., Cuesta-Rubio, O., De Martin, S., Carrara, M., 2020b. The Cuban propolis component nemorosone inhibits proliferation and metastatic properties of human colorectal cancer cells. Int. J. Mol. Sci. 21 https://doi.org/10.3390/ijms21051827.

Gabbia, D., Carpi, S., Sarcognato, S., Zanotto, I., Sayaf, K., Colognesi, M., Polini, B., Digiacomo, M., Macchia, M., Nieri, P., Carrara, M., Cazzagon, N., Russo, F.P., Guido, M., De Martin, S., 2023. The phenolic compounds tyrosol and hydroxytyrosol counteract liver fibrogenesis via the transcriptional modulation of NADPH oxidases and oxidative stress-related miRNAs. Biomed. Pharmacother. 157 https://doi.org/10.1016/j.biopha.2022.114014.

Gabbia, D., Roverso, M., Guido, M., Sacchi, D., Scaffidi, M., Carrara, M., Orso, G., Russo, F.P., Floreani, A., Bogialli, S., De Martin, S., 2019. Western diet-induced metabolic alterations affect circulating markers of liver function before the development of steatosis. Nutrients 11. https://doi.org/10.3390/nu11071602.

Gabbia, D., Saponaro, M., Sarcognato, S., Guido, M., Ferri, N., Carrara, M., De Martin, S., 2020. Fucus vesiculosus and ascophyllum nodosum ameliorate liver function by reducing diet-induced steatosis in rats. Mar. Drugs 18. https://doi.org/10.3390/md18010062.

Ghosh, P., Sasaki, K., Pulido Ruiz, I.A., King, K.E., Weinman, S.A., Wozniak, A.L., 2023. Inflammatory macrophage to hepatocyte signals can be prevented by extracellular vesicle reprogramming. J. Cell Sci. 136, jcs260691. https://doi.org/10.1242/jcs.260691.

Gori, M., Giannitelli, S.M., Zancla, A., Mozetic, P., Trombetta, M., Merendino, N., Rainer, A., 2021. Quercetin and hydroxytyrosol as modulators of hepatic steatosis: a NAFLD-on-a-chip study. Biotechnol. Bioeng. 118, 142–152. https://doi.org/10.1002/bit.27557.

Hamid, O., Eltelbany, A., Mohammed, A., Alsabbagh Alchirazi, K., Trakroo, S., Asaad, I., 2022. The epidemiology of non-alcoholic steatohepatitis (NASH) in the United States between 2010-2020: a population-based study. Ann. Hepatol. 27, 100727 https://doi.org/10.1016/j.aohep.2022.100727.

Huang, D.Q., El-Serag, H.B., Loomba, R., 2021. Global epidemiology of NAFLD-related HCC: trends, predictions, risk factors and prevention. Nat. Rev. Gastroenterol. Hepatol. 18, 223–238. https://doi.org/10.1038/s41575-020-00381-6.

Huang, Y., Li, S., Han, Z., Du, J., Liu, Xin, Zhu, Z., Zheng, L., Han, S., Shi, H., Wang, X., Liu, Xinmei, Jiang, Z., Li, Y., Li, X., Gu, X., Han, D., Li, D., 2022. Tyrosol ameliorates liver inflammatory response in a mouse model of nonalcoholic fatty liver disease (NFALD) by regulating JAK1/STAT3. Nat. Prod. Commun. 17, 1934578X221111033 https://doi.org/10.1177/1934578X221111033.

Huby, T., Gautier, E.L., 2022. Immune cell-mediated features of non-alcoholic steatohepatitis. Nat. Rev. Immunol. 22, 429–443. https://doi.org/10.1038/s41577-021-00639-3.

Kelm, J.M., Timmins, N.E., Brown, C.J., Fussenegger, M., Nielsen, L.K., 2003. Method for generation of homogeneous multicellular tumor spheroids applicable to a wide variety of cell types. Biotechnol. Bioeng. 83, 173–180. https://doi.org/10.1002/bit.10655.

Kim, Y.-Y., Lee, S., Kim, M.-J., Kang, B.-C., Dhakal, H., Choi, Y.-A., Park, P.-H., Choi, H., Shin, T.-Y., Choi, H.G., Kwon, T.K., Khang, D., Kim, S.-H., 2017. Tyrosol attenuates lipopolysaccharide-induced acute lung injury by inhibiting the inflammatory response and maintaining the alveolar capillary barrier. Food Chem. Toxicol. 109, 526–533. https://doi.org/10.1016/j.fct.2017.09.053.

Kisseleva, T., Brenner, D., 2021. Molecular and cellular mechanisms of liver fibrosis and its regression. Nat. Rev. Gastroenterol. Hepatol. 18, 151–166. https://doi.org/10.1038/s41575-020-00372-7.

Kraeuter, A.-K., Guest, P.C., Sarnyai, Z., 2019. The open field test for measuring locomotor activity and anxiety-like behavior. Methods Mol. Biol. 1916, 99–103. https://doi.org/10.1007/978-1-4939-8994-2_9.

Majzoub, A.M., Nayfeh, T., Barnard, A., Munaganuru, N., Dave, S., Singh, S., Murad, M. H., Loomba, R., 2021. Systematic review with network meta-analysis: comparative efficacy of pharmacologic therapies for fibrosis improvement and resolution of NASH. Aliment. Pharmacol. Ther. 54, 880–889. https://doi.org/10.1111/apt.16583.

Mateos, R., Sarria, B., Bravo, L., 2020. Nutritional and other health properties of olive pomace oil. Crit. Rev. Food Sci. Nutr. 60, 3506–3521. https://doi.org/10.1080/10408398.2019.1698005.

Mihm, S., 2018. Danger-associated molecular patterns (DAMPs): molecular triggers for sterile inflammation in the liver. Indian J. Manag. Sci. 19, 3104. https://doi.org/10.3390/ijms19103104.

Mohammed, S., Thadathil, N., Selvarani, R., Nicklas, E.H., Wang, D., Miller, B.F., Richardson, A., Deepa, S.S., 2021. Necroptosis contributes to chronic inflammation and fibrosis in aging liver. Aging Cell 20, e13512. https://doi.org/10.1111/acel.13512.

Mosca, A., Crudele, A., Smeriglio, A., Braghini, M.R., Panera, N., Comparcola, D., Alterio, A., Sartorelli, M.R., Tozzi, G., Raponi, M., Trombetta, D., Alisi, A., 2021. Antioxidant activity of Hydroxytyrosol and Vitamin E reduces systemic inflammation in children with paediatric NAFLD. Dig. Liver Dis. 53, 1154–1158. https://doi.org/10.1016/j.dld.2020.09.021.

Paramita Pal, P., Sajeli Begum, A., Ameer Basha, S., Araya, H., Fujimoto, Y., 2023. New natural pro-inflammatory cytokines (TNF-α, IL-6 and IL-1β) and iNOS inhibitors identified from Penicillium polonicum through in vitro and in vivo studies. Int. Immunopharm. 117, 109940 https://doi.org/10.1016/j.intimp.2023.109940.

Pearlman, M., Loomba, R., 2014. State of the art: treatment of nonalcoholic steatohepatitis. Curr. Opin. Gastroenterol. 30, 223. https://doi.org/10.1097/MOG.0000000000000060.

Piccinini, F., Tesei, A., Arienti, C., Bevilacqua, A., 2015. Cancer multicellular spheroids: volume assessment from a single 2D projection. Comput. Methods Progr. Biomed. 118, 95–106. https://doi.org/10.1016/j.cmpb.2014.12.003.

Pirozzi, C., Lama, A., Simeoli, R., Paciello, O., Pagano, T.B., Mollica, M.P., Di Guida, F., Russo, R., Magliocca, S., Canani, R.B., Raso, G.M., Calignano, A., Meli, R., 2016. Hydroxytyrosol prevents metabolic impairment reducing hepatic inflammation and restoring duodenal integrity in a rat model of NAFLD. J. Nutr. Biochem. 30, 108–115. https://doi.org/10.1016/j.jnutbio.2015.12.004.

Qu, B., Liu, X., Liang, Y., Zheng, K., Zhang, C., Lu, L., 2022. Salidroside in the treatment of NAFLD/NASH. Chem. Biodivers. 19, e202200401 https://doi.org/10.1002/cbdv.202200401.

Rinella, M.E., Lazarus, J.V., Ratziu, V., Francque, S.M., Sanyal, A.J., Kanwal, F., Romero, D., Abdelmalek, M.F., Anstee, Q.M., Arab, J.P., Arrese, M., Bataller, R., Beuers, U., Boursier, J., Bugianesi, E., Byrne, C., Narro, G.E.C., Chowdhury, A., Cortez-Pinto, H., Cryer, D., Cusi, K., El-Kassas, M., Klein, S., Eskridge, W., Fan, J., Gawrieh, S., Guy, C.D., Harrison, S.A., Kim, S.U., Koot, B., Korenjak, M., Kowdley, K., Lacaille, F., Loomba, R., Mitchell-Thain, R., Morgan, T.R., Powell, E., Roden, M., Romero-Gómez, M., Silva, M., Singh, S.P., Sookoian, S.C., Spearman, C.

W., Tiniakos, D., Valenti, L., Vos, M.B., Wong, V.W.-S., Xanthakos, S., Yilmaz, Y., Younossi, Z., Hobbs, A., Villota-Rivas, M., Newsome, P.N., Ajmeral, V., Alazawi, W., Alkhatry, M., Alkhouri, N., Allen, A., Allison, M., Alswat, K., Alvares-da-Silva, M.R., Alves-Bezerra, M., Armstrong, M.J., Arufe, D., Aschner, P., Baffy, G., Bansal, M., Bedossa, P., Belfort, R., Berg, T., Berzigotti, A., Betel, M., Bianco, C., Brass, C., Brosgart, C.L., Brunt, E.M., Buti, M., Caldwell, S., Carr, R., Casanovas, T., Castera, L., Caussy, C., Cerda, E., Chalasani, N., Chan, W.K., Charatcharoenwitthaya, P., Charlton, M., Cheung, A., Chiodi, D., Chung, R., Cohen, D., Corey, K., Cotrim, H.P., Crespo, J., Dassanayake, A., Davidson, N., Knegt, R.D., Ledinghen, V.D., Demir, M., Diaz, S., Diehl, A.M., Dimmig, B., Dirchwolf, M., Duseja, A., Dvorak, K., Ekstedt, M., Wakil, R.E., Ferraz, M.L., Friedman, S., Fuchs, M., Gastaldelli, A., Geerts, A., Geier, A., Girala, M., Goh, G., Goossens, N., Graupera, I., Hagström, H., Henry, Z., Hunyady, B., Hutchison, A., Isaacs, S., Jornayvaz, F., Kemp, C., Kile, D., Kim, W., Kleiner, D., Kohli, R., Kugelmas, M., Lavine, J., Lazo, M., Leite, N., Lozano, A., Luukkonen, P., Macedo, P., Mansour, D., Mantzoros, C., Marchesini, G., Marciano, S., Martinez, K., Mateva, L.V., Mato, J.M., McCary, A., Miele, L., Mikolasevic, I., Miller, V., Moreno, R., Moylan, C., Nakajima, A., Nault, J.C., Norris, S., Noureddin, M., Oliveira, C.P., Ong, A., Padilla, M., Pais, R., Panduro, A., Panigrahi, M.K., Papatheodoridis, G., Pelusi, S., Pérez, M., Escobar, J.P., Perseghin, G., Pessoa, M., Petta, S., Pinzani, M., Lupsor, M.P., Rabiee, A., Romeo, S., Rotman, Y., Rowe, I., Salupere, R., Satapathy, S., Schattenberg, J.M., Schaufert, W., Schnabl, B., Seim, L., Serfaty, L., Shapiro, D., Singal, A.K., Skladany, L., Stefan, N., Stine, J., Sundaram, S., Svegliati-Baroni, G., Szabo, G., Tacke, F., Tanwandee, T., Targher, G., Terrault, N., Tetri, B., Thiele, M., Tisthammer, B., Delgadillo, A.T., Trauner, M., Tsochatzis, E., Kleef, L.V., Mil, S.V., VanWagner, L., Velasco, J.A.V.R., Vesterhus, M., Vilar-Gomez, E., Watt, K., Wattacheril, J., Wilkins, F., Willemse, J., Zekry, A., Zelber-Sagi, S., 2023. A multi-society Delphi consensus statement on new fatty liver disease nomenclature. J. Hepatol. 0 https://doi.org/10.1016/j.jhep.2023.06.003.

Sarna, L.K., Sid, V., Wang, P., Siow, Y.L., House, J.D., O, K., 2016. Tyrosol attenuates high fat diet-induced hepatic oxidative stress: potential involvement of cystathionine β-synthase and cystathionine γ-lyase. Lipids 51, 583–590. https://doi.org/10.1007/s11745-015-4084-y.

Sica, A., Invernizzi, P., Mantovani, A., 2014. Macrophage plasticity and polarization in liver homeostasis and pathology. Hepatology 59, 2034–2042. https://doi.org/10.1002/hep.26754.

Stepanova, M., Henry, L., Younossi, Z.M., 2023. Economic burden and patient-reported outcomes of nonalcoholic fatty liver disease. Clinics in Liver Disease, Update on Non-Alcoholic Steatohepatitis 27, 483–513. https://doi.org/10.1016/j.cld.2023.01.007.

Sutti, S., Albano, E., 2020. Adaptive immunity: an emerging player in the progression of NAFLD. Nat. Rev. Gastroenterol. Hepatol. 17, 81–92. https://doi.org/10.1038/s41575-019-0210-2.

Todoric, J., Di Caro, G., Reibe, S., Henstridge, D.C., Green, C.R., Vrbanac, A., Ceteci, F., Conche, C., McNulty, R., Shalapour, S., Taniguchi, K., Meikle, P.J., Watrous, J.D., Moranchel, R., Najhawan, M., Jain, M., Liu, X., Kisseleva, T., Diaz-Meco, M.T., Moscat, J., Knight, R., Greten, F.R., Lau, L.F., Metallo, C.M., Febbraio, M.A., Karin, M., 2020. Fructose stimulated de novo lipogenesis is promoted by inflammation. Nat. Metab. 2, 1034–1045. https://doi.org/10.1038/s42255-020-0261-2.

Wu, K., Qian, Q., Zhou, J., Sun, D., Duan, Y., Zhu, X., Sartorius, K., Lu, Y., 2023. Regulatory T cells (Tregs) in liver fibrosis. Cell Death Dis. 9, 53. https://doi.org/10.1038/s41420-023-01347-8.

Xi, S., Zheng, X., Li, X., Jiang, Y., Wu, Y., Gong, J., Jie, Y., Li, Z., Cao, J., Sha, L., Zhang, M., Chong, Y., 2021. Activated hepatic stellate cells induce infiltration and formation of CD163+ macrophages via CCL2/CCR2 pathway. Front. Med. 8, 627927 https://doi.org/10.3389/fmed.2021.627927.

Xiao, Z., Liu, M., Yang, F., Liu, G., Liu, J., Zhao, W., Ma, S., Duan, Z., 2023. Programmed cell death and lipid metabolism of macrophages in NAFLD. Front. Immunol. 14.

Yankelevitch-Yahav, R., Franko, M., Huly, A., Doron, R., 2015. The forced swim test as a model of depressive-like behavior. J. Vis. Exp. 52587 https://doi.org/10.3791/52587.

Younossi, Z., Anstee, Q.M., Marietti, M., Hardy, T., Henry, L., Eslam, M., George, J., Bugianesi, E., 2017. Global burden of NAFLD and NASH: trends, predictions, risk factors and prevention. Nature Reviews Gastroenterology & Hepatology 15, 11.

Younossi, Z., Stepanova, M., Ong, J.P., Jacobson, I.M., Bugianesi, E., Duseja, A., Eguchi, Y., Wong, V.W., Negro, F., Yilmaz, Y., Romero-Gomez, M., George, J., Ahmed, A., Wong, R., Younossi, I., Ziayee, M., Afendy, A., 2019. Nonalcoholic steatohepatitis is the fastest growing cause of hepatocellular carcinoma in liver transplant candidates. Clin. Gastroenterol. Hepatol. 17, 748–755.e3. https://doi.org/10.1016/j.cgh.2018.05.057.

Younossi, Z.M., Stepanova, M., Ong, J., Trimble, G., AlQahtani, S., Younossi, I., Ahmed, A., Racila, A., Henry, L., 2021. Nonalcoholic steatohepatitis is the most rapidly increasing indication for liver transplantation in the United States. Clin. Gastroenterol. Hepatol. 19, 580–589.e5. https://doi.org/10.1016/j.cgh.2020.05.064.

Zhang, G., Wang, X., Chung, T.-Y., Ye, W., Hodge, L., Zhang, L., Chng, K., Xiao, Y.-F., Wang, Y.J., 2020. Carbon tetrachloride (CCl4) accelerated development of non-alcoholic fatty liver disease (NAFLD)/steatohepatitis (NASH) in MS-NASH mice fed western diet supplemented with fructose (WDF). BMC Gastroenterol. 20, 339. https://doi.org/10.1186/s12876-020-01467-w.

Zhao, W., Wei, H., Lu, J., Sha, W., Sun, D., Pan, T., Lei, T., 2023. Tyrosol attenuates lipopolysaccharide-induced inflammation in HUVECs to promote vascular health against atherosclerosis challenge. Exp. Ther. Med. 25, 240. https://doi.org/10.3892/etm.2023.11939.

Zhou, Y., Zhang, H., Yao, Y., Zhang, X., Guan, Y., Zheng, F., 2022. CD4+ T cell activation and inflammation in NASH-related fibrosis. Front. Immunol. 13, 967410 https://doi.org/10.3389/fimmu.2022.967410.